Physica Medica 78 (2020) 201–208

Contents lists available at ScienceDirect

Physica Medica

journal homepage: www.elsevier.com/locate/ejmp

Original paper

Automated classification of urinary stones based on microcomputed tomography images using convolutional neural network

Leni Aziyus Fitri[a,b], Freddy Haryanto[b], Hidetaka Arimura[c,*], Cui YunHao[d], Kenta Ninomiya[d], Risa Nakano[d], Mohammad Haekal[e], Yuni Warty[b], Umar Fauzi[b]

[a] Department of Radiology, Baiturrahmah University, By pass km 15 Aie Pacah, Padang, West Sumatra 25172, Indonesia
[b] Department of Physics, Institut Teknologi Bandung, Jl. Ganesa No. 10, Bandung, West Java 40132, Indonesia
[c] Faculty of Medical Sciences, Kyushu University, 3-1-1, Maidashi, Higashi-ku, Fukuoka 812-8582, Japan
[d] Graduate School of Medical Sciences, Kyushu University, 3-1-1, Maidashi, Higashi-ku, Fukuoka 812-8582, Japan
[e] Department of Physics, Faculty of Sciences and Data Analytics, Institut Teknologi Sepuluh Nopember, Kampus ITS Sukolilo, Surabaya, East Java 60111, Indonesia

ARTICLE INFO

Keywords:
Convolutional neural network
Energy dispersive X-ray spectra
Micro-CT
Urinary stones

ABSTRACT

Purpose: The classification of urinary stones is important prior to treatment because the treatments depend on three types of urinary stones, i.e., calcium, uric acid, and mixture stones. We have developed an automatic approach for the classification of urinary stones into the three types based on microcomputed tomography (micro-CT) images using a convolutional neural network (CNN).

Materials and methods: Thirty urinary stones from different patients were scanned *in vitro* using micro-CT (pixel size: 14.96 μm; slice thickness: 15 μm); a total of 2,430 images (micro-CT slices) were produced. The slices (227 × 227 pixels) were classified into the three categories based on their energy dispersive X-ray (EDX) spectra obtained via scanning electron microscopy (SEM). The images of urinary stones from each category were divided into three parts; 66%, 17%, and 17% of the dataset were assigned to the training, validation, and test datasets, respectively. The CNN model with 15 layers was assessed based on validation accuracy for the optimization of hyperparameters such as batch size, learning rate, and number of epochs with different optimizers. Then, the model with the optimized hyperparameters was evaluated for the test dataset to obtain classification accuracy and error.

Results: The validation accuracy of the developed approach with CNN with optimized hyperparameters was 0.9852. The trained CNN model achieved a test accuracy of 0.9959 with a classification error of 1.2%.

Conclusions: The proposed automated CNN-based approach could successfully classify urinary stones into three types, namely calcium, uric acid, and mixture stones, using micro-CT images.

1. Introduction

Urinary stone disease is caused by the accumulation of solid mineral materials in the kidney, ureter, or bladder [1]. In the last seven years, its prevalence has increased in both developing and developed countries [2,3]. In particular, from 2007 to 2013, the National Health and Nutrition Examination Survey (NHANES) indicated that the prevalence of urinary stones has almost doubled from 3.9% to 7.5% in females aged 20–39 years, while it has remained stable at 17.8% in males older than 60 years [4]. In addition, Kittanamongkolchai reported that the incidence of kidney stones of unknown chemical compositions also increased between 1984 and 2012[5].

Treatment methods for the removal of urinary stones from patient bodies are determined based on the type of urinary stones, including those primarily formed of calcium, uric acid, or a mixture of both [8]. Each type of urinary stone has a different chemical composition; for example, calcium urinary stones are typically formed of CaC_2O_4 or $Ca_{10}(PO_4)_6(OH)_2$, uric acid stones are formed of $C_5H_4N_4O_3$ (uric acid), and Ca and struvite (i.e., $MgNH_4PO_46H_2O$) might be present in the mixture stones [1,6,7]. Based on the type of urinary stone, several clinical treatment methods are available: percutaneous nephrolithotomy (PCNL) and retrograde intrarenal surgery (RIRS) are used to remove calcium stones, while uric acid stones that have low density can be eliminated via oral chemolysis (alkalization of urine) [9]; mixture stones can be removed via extracorporeal shockwave lithotripsy (ESWL) [10].

* Corresponding author at: Division of Medical Quantum Science, Department of Health Sciences, Faculty of Medical Sciences, Kyushu University, 3-1-1, Maidashi, Higashi-ku, Fukuoka 812-8582, Japan.
E-mail address: arimurah@med.kyushu-u.ac.jp (H. Arimura).

https://doi.org/10.1016/j.ejmp.2020.09.007
Received 2 March 2020; Received in revised form 2 August 2020; Accepted 3 September 2020
Available online 08 October 2020

Thus, it is necessary to determine the composition of urinary stones before a treatment method can be applied. Manual classification approaches for urinary stones based on their chemical compositions using conventional computerized tomography (CT) images have been reported in several works [11–15]. However, these manual approaches are time consuming and are susceptible to intra- and interobserver variabilities during classification. Consequently, there is a need for automated approaches for urinary stone classification to ensure appropriate selection of treatment methods.

Several previous works have reported on automated detection approaches for urinary stones that employ machine learning techniques including deep learning [16–21]. Black et al. showed that deep learning could be used to detect kidney stone composition [16], while Lankvist et al. reported on the automated detection of ureteral stones in conventional CT images using convolutional neural networks (CNNs) [17]. Parakh et al. evaluated the performance of two pretrained CNN models, which were used to detect urinary stones in conventional CT images [3]. Furthermore, Xiang et al. proposed three CNN models to detect urine calcium oxalate crystallization [18]. Kazemi et al. developed an automated approach for the detection of kidney stones in patients via ensemble learning [19]. Moreover, Chaitanya et al. proposed an approach for the detection of chronic kidney disease using artificial neural networks and a gravitational search algorithm [20]. Perrot et al. showed that radiomics and machine learning enabled accurate detection of kidney stones in patients [21].

Previous work used machine learning techniques [16–21], including those based on deep learning, to obtain promising results (developed machine learning and CNN model) for the detection of urinary stones alone; however, to the best of our knowledge, no previous work has presented automated approaches for simultaneous classification of all three types of urinary stones. Such an approach could require high-quality images for analysis such as micro-CT images. In particular, micro-CT is an X-ray modality that involves a small focal spot (e.g., < 5 μm) with pixel sizes and slice thicknesses on the micrometer scale (e.g., 14.96 μm and 15 μm, respectively) [22–24]. Hence, the objective of this study was to develop an automated approach for classification of urinary stones into three types (namely, calcium, uric acid, and mixture stones) using micro-CT images via deep learning.

2. Materials and methods

2.1. Data preparation

Thirty patients (median age: approximately 40 and 60 years; age range: 38–71 years), who underwent surgical removal of urinary stones participated in this study under the approval of the Hasan Sadikin Hospital, Indonesia. Data preparation for this study consisted of two steps, as shown in Fig. 1. First, urinary stones were scanned via micro-CT (SkyScan 1173, Bruker, Germany). Then, micro-CT projection images of each stone were reconstructed using software (Nrecon 1.7.1.0, Bruker micro CT). This step yielded 2430 micro-CT slice images of the urinary stones.

According to a paper of Fitri et al. [25], the method to optimize the acquisition and reconstruction parameters for urinary stones using micro-CT is based on signal-to-noise ratio (SNR). Five urinary stones with a diameter of 5–15 mm were scanned with eight source voltages (45, 55, 65,…, 115) kV. Region of interest (ROI) was drawn in the two-dimensional (2D) urinary stone image by referring to the homogeneous area. To calculate the SNR of the image, the mean hounsfield unit value was divided by standard deviation in ROI. The optimized acquisition and reconstruction parameters were the parameter which obtained the high SNR of the image [25]. The optimized acquisition and reconstruction parameters for the scanned urinary stones using micro-CT are listed in Table 1 [25].

Second, the stones were classified into the three types of urinary stones. Table 2 lists the acquisition parameters for the EDX SEM (JSM-6510LV, JEOL, Japan) measurements. In particular, the classification method adopted for urinary stones is based on the intensities and energies of the characteristic X-ray peaks obtained, which are determined by their chemical compositions [26,27]. Fig. 2 shows the reference EDX spectra for pure calcium oxalate (CaC_2O_4) and uric acid powder ($C_5H_4N_4O_3$), which, as specified previously, are primary components in two types of urinary stones.

2.2. Automated classification

A CNN is a pattern recognition network that can learn characteristics about data from already available large datasets. Therefore, a large dataset is necessary to obtain an effective model using CNNs. This dataset includes micro-CT slice images; some examples of these images are shown in Fig. 3. Table 3 lists the distribution of these micro-CT slice images based on the type of urinary stone.

The dataset was divided into three sets (training, validation, and test) to avoid overlapping sets. In particular, the training dataset was used to build the CNN model [28], the validation dataset was employed to evaluate the developed model [29–31], and the performance of the model was evaluated using the independent test dataset [28].

CNN architecture was used for automated classification of micro-CT images in our study, because previous studies showed that CNN was the most successful network for medical image classification tasks [32–36]. According to a review paper by Langkvist et al. [17], CNN uses local receptive fields, shared weights, and often spatial down-sampling. Therefore, the CNN can reduce the number of parameters, lead to savings in memory requirements, computation complexity, and increasing the network's generalization performance [17]. CNN is the optimal choice for classification based on image recognition. The network convolved and filtered each pixel value of the image. The micro CT can produce the high-quality images (the micrometer pixel size of image). Therefore, we also have chosen the CNN for classifying the micro-CT image. In particular, the CNN architecture employed in our work included 15 layers and is illustrated in Fig. 4. The 15 CNN layers include three convolution two-dimensional (2D) layers, three batch normalization layers, three rectified linear unit (ReLu) layers, three max-pooling layers, a fully connected layer, a softmax layer, and a classification layer. The kernel sizes in the convolution and max-pooling layers were 3 × 3 and 2 × 2, respectively.

Fig. 5 shows a flowchart for the automated classification of urinary stone images into the three types of urinary stones. This approach was implemented in MATLAB 2019a on a system with a deep learning server (NVIDIA GP102GL, Quadro P6000, 24 GB 384 bit). The training and validation datasets were augmented for training by applying geometric transformations such as rotation (-20° to 20°) and translation (-3 to 3 pixels in the x and y directions) to improve model generalization. It should be noted that this augmentation was also performed in a previous study [3]. The leave-one-out cross validation test may be used for small datasets like our study. However, the cross-validation test has an issue that reusing a holdout set adaptively multiple times can easily lead to overfitting to the holdout set itself [37]. For this reason, we adopted an approach based on an independent test dataset as shown in Fig. 5 according the Transparent Reporting of a multivariable prediction model for Individual Prognosis or Diagnosis (TRIPOD) statement [38].

The hyperparameters of the proposed CNN model, such as initial learning rate, batch size, epoch, and L2 regularization, were optimized with different optimizers. In particular, optimization was performed using the stochastic gradient descent with momentum (SGDM), derivation of adaptive moment estimation (Adam), and root mean square propagation (Rmsprop) approaches. The L2 regularization and epoch were set as 0.1 and 30, respectively, while the learning rate was changed from 0.00001 to 0.01 by a factor of 10. The batch sizes were 16, 32, 64, and 128.

The root mean squared error (RMSE) [28], which was used for

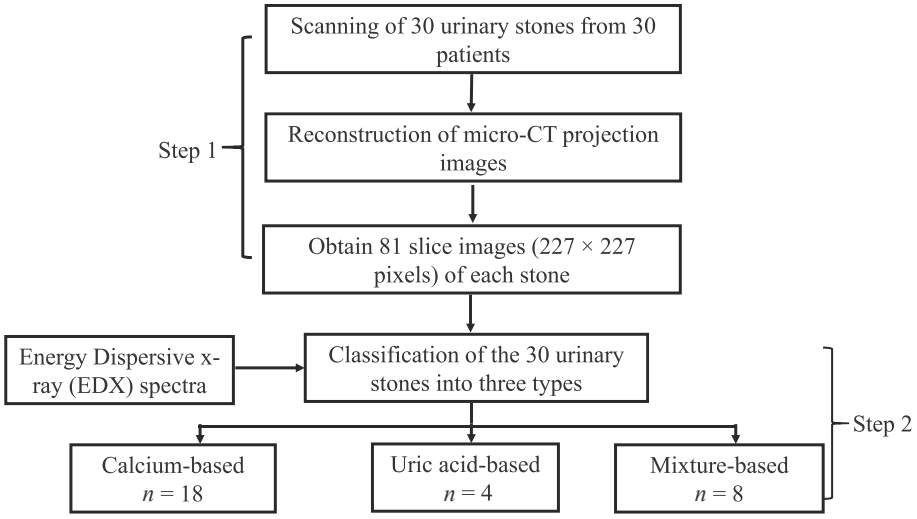

Fig. 1. Flowchart for the data preparation process adopted in our study; n = number of stones.

Table 1
Optimized Acquisition and Reconstruction Parameters for Urinary Stones using micro-CT.

Acquisition	
Source voltage (kV)	75
Source current (μA)	106
Image pixel size (μm)	14.96
Filter	Al (1 mm)
Exposure time (ms)	600
Rotation step (deg)	0.2
Slice thickness (μm)	15
Reconstruction	
Ring artifact correction	15
Beam hardening correction (%)	8
Smoothing	1

Table 2
Acquisition Parameters for Urinary Stones using EDX SEM.

Source voltage	15 kV
Magnification	500x
Probe current	1nA

hyperparameter optimization in the CNN model during classification for the training and validation datasets, was calculated as follows:

$$RMSE = \sqrt{\frac{1}{n}\sum_{i=1}^{n}(y_i - \hat{f}(x_i))^2}. \quad (1)$$

Thus, the RMSE metric is a function of model residuals, where n, y_i, $\hat{f}(x_i)$ are number of epochs, training observation, the prediction, respectively. We define $y_i - \hat{f}(x_i)$ the prediction error for the test observations. We assumed that the optimal model is the one with the smallest RMSE for training and validation datasets and has the smallest difference between training and validation datasets for a specific epochideally, the validation RMSE should be almost equal to the training RMSE [29].

3. Results

3.1. Hyperparameter optimization

Fig. 6 shows the relationships between CNN classification accuracy and learning rate for different batch sizes for the validation and test datasets. It can be observed from Fig. 6a that all CNN models with batch sizes of 16, 32, 64, and 128 had accuracies higher than 0.9 at a learning rate of 0.00001 for the validation dataset. However, the CNN attained the best accuracy of 0.9959 for the test dataset with a batch size of 32 at a learning rate of 0.00001 with an SGDM optimizer (Fig. 6b).

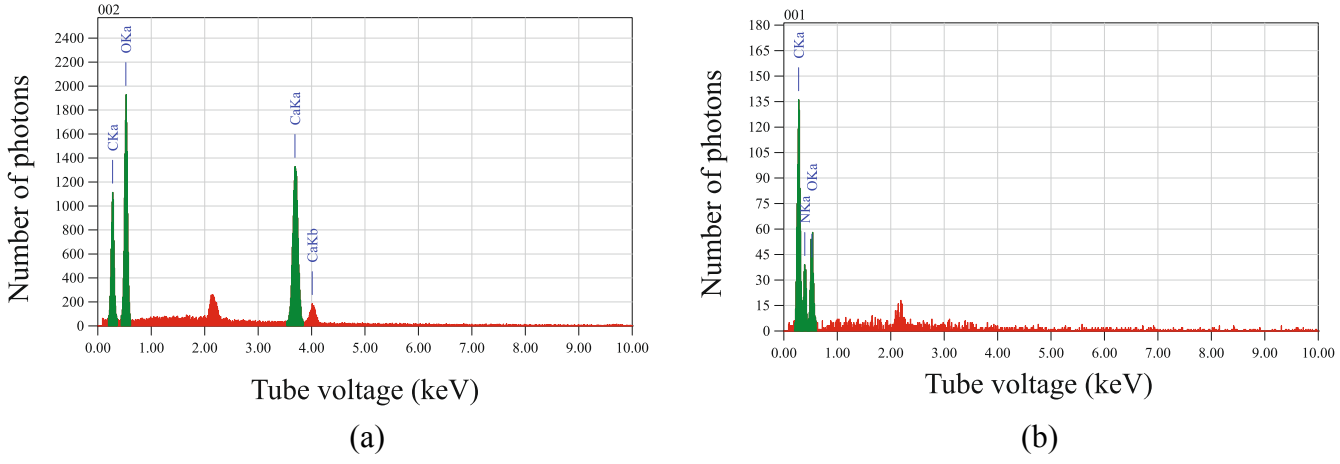

Fig. 2. Reference EDX spectra for pure calcium oxalate (a) calcium oxalate (CaC_2O_4) and (b) uric acid powder ($C_5H_4N_4O_3$).

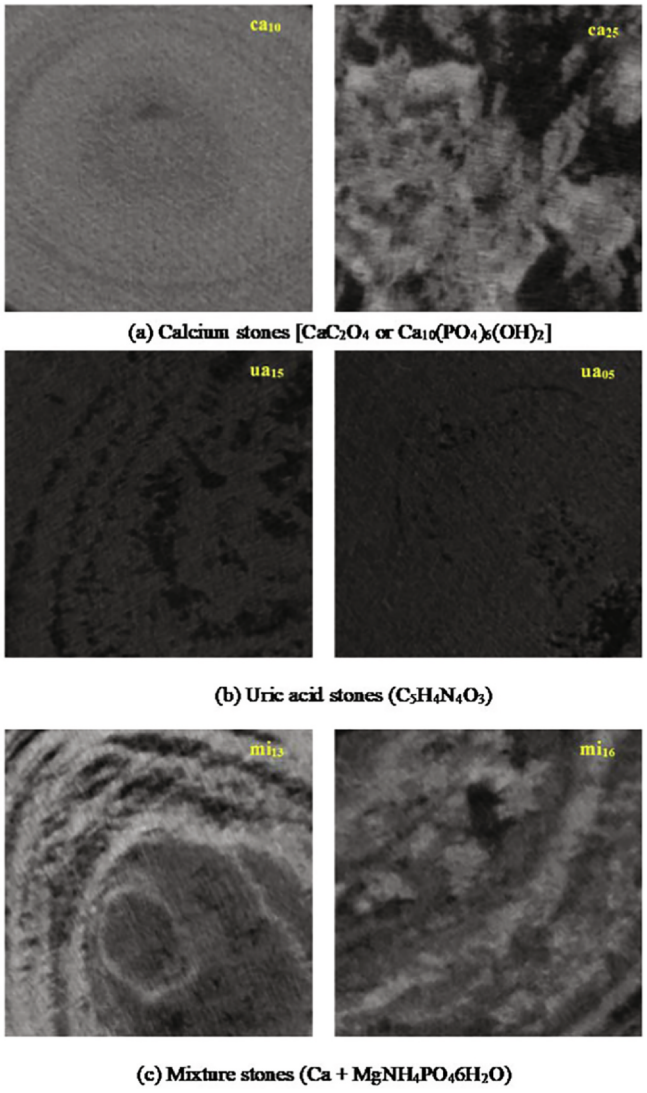

Fig. 3. Examples of micro-CT slice images of the three types of urinary stones.

Table 3
Distribution of micro-CT slice images based on three types of urinary stone.

	Calcium		Uric acid		Mixture	
	Number of stones	Number of slice images	Number of stones	Number of slice images	Number of stones	Number of slice images
Training	12	972	2	162	6	486
Validation	3	243	1	81	1	81
Test	3	243	1	81	1	81

Fig. 7 shows the relationships between CNN classification accuracies and batch size as a parameter of three optimizers (SGDM, Adam, and Rmsprop) at a learning rate of 0.00001 for the validation and test datasets. The accuracy of the SGDM solver was highest among the solvers with a learning rate of 0.00001 and batch size of 32 for the test dataset.

Figs. 8 and 9 show RMSEs as a function of the number of epochs for the validation and training datasets using optimized hyperparameters for a batch size of 32 and learning rate of 0.00001 with an SGDM optimizer. Regarding the training progress, validation loss, training loss, validation, and test accuracy, the optimized hyperparameters were a solver of SGDM, batch size of 32, and learning rate of 0.00001. Note that the number of epochs influenced the optimized hyperparameters.

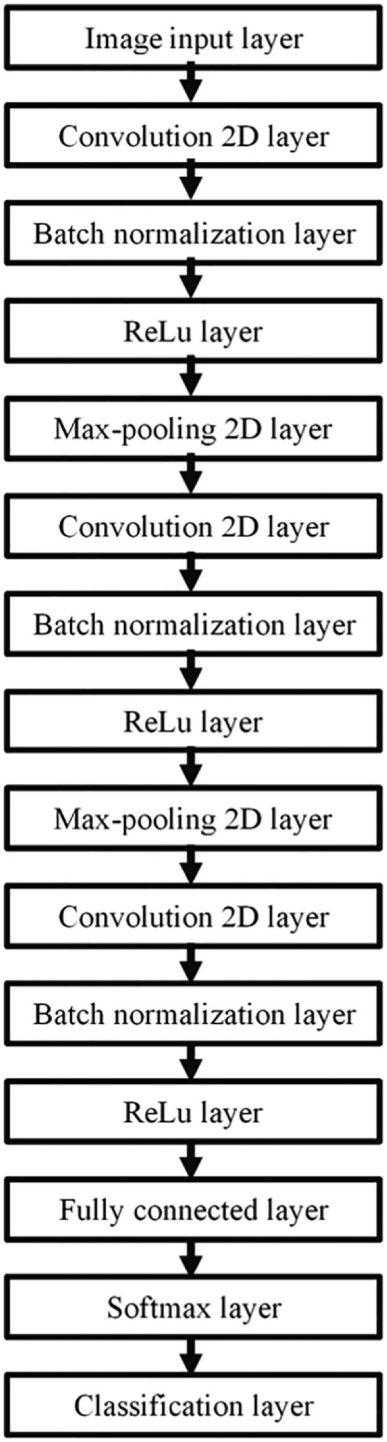

Fig. 4. CNN architecture with the 15 layers used in this study.

Fig. 8 indicates the optimized number of epochs whereas Fig. 9 is overfitted after 30 epochs.

3.2. Test accuracy and confusion matrix

Table 4 shows the confusion matrix for the automated classification of urinary stones into the three types, namely calcium, mixture, and uric acid stones. A test accuracy of 0.9959 was realized for the classification with an error of 1.2%.

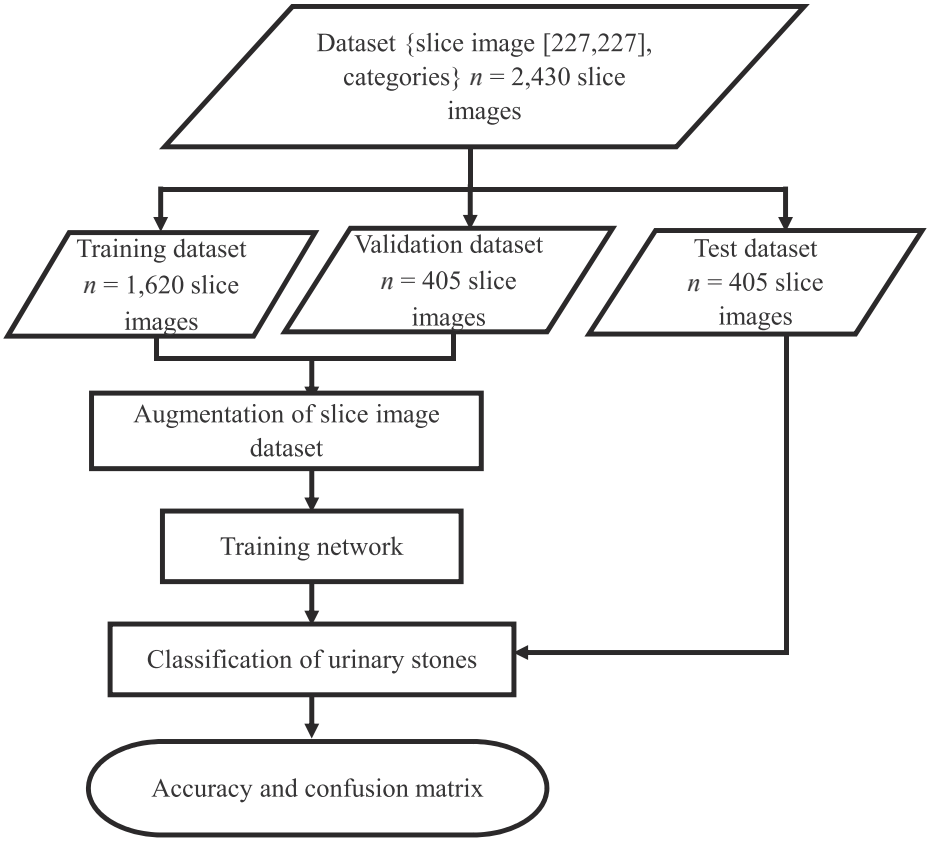

Fig. 5. Flowchart of the automated classification process for urinary stones using micro-CT slice images.

4. Discussion

A CNN-based automated classification approach for urinary stones using micro-CT images was proposed, which has a classification accuracy of 0.9959. Compared with previous works in which only a CNN-based algorithm was used to detect ureteral stones [17], our proposed approach could classify urinary stones into three types, namely calcium, uric acid, and mixture stones. Furthermore, our proposed approach obtained more representative results than trained support vector machine (SVM)-based algorithms because the raw pixels [ROI with 227 × 227 pixels] of the extracted features were used as input for the CNN model. In another previous study, while their proposed SVM-based algorithm for automatic classification of urinary stones resulted in 100% sensitivity and 100% specificity for six spectra obtained using Raman spectroscopy, background correction and a large number of measurement spots on the sample surface were essential for appropriate classification results [39].

Our proposed automated approach for urinary stone classification has several advantages compared with conventional methods. First, the automated approach reduced the time required to classify urinary stones compared to conventional methods. Second, urinary stone analysis using infrared spectroscopy (FT-IR), XRD, and transmission electron microscopy (TEM) requires no prior preparation of samples [10]. Third, the proposed automated approach could be used to determine

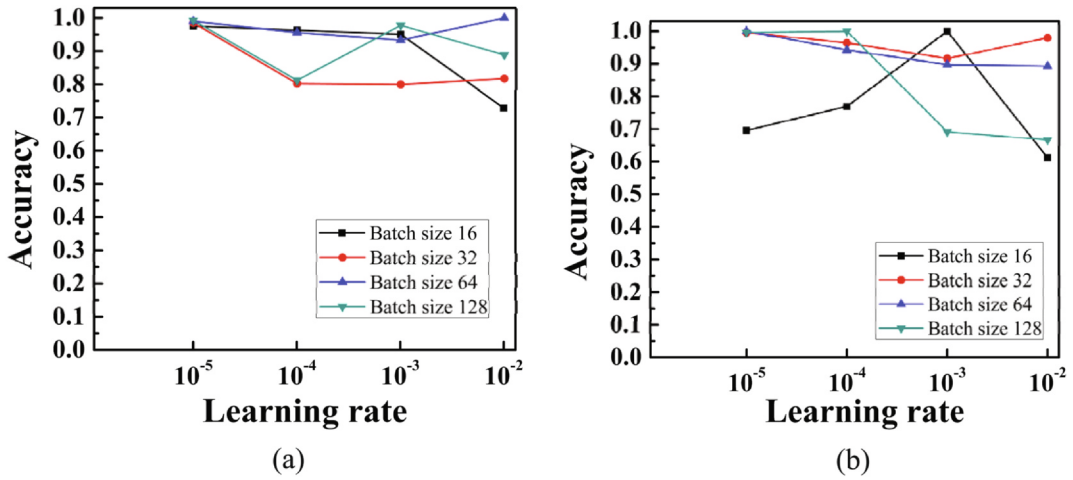

Fig. 6. Relationship between CNN classification accuracy and learning rate for different batch sizes (16, 32, 64, and 128) with an SGDM optimizer for (a) validation and (b) test datasets.

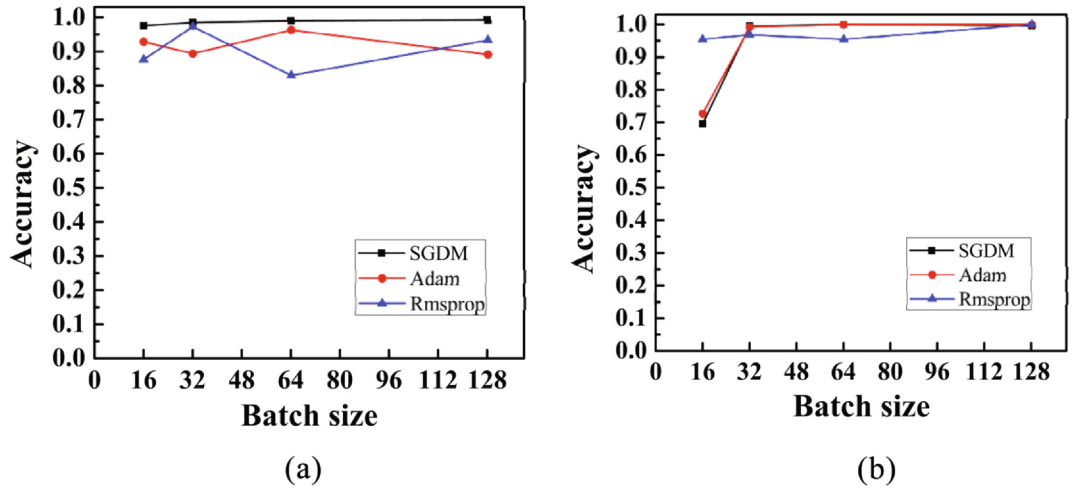

Fig. 7. Relationship between CNN classification accuracy and batch size for three different optimizers (SGDM, Adam, and Rmsprop) at a learning rate of 0.00001 for (a) validation and (b) test datasets.

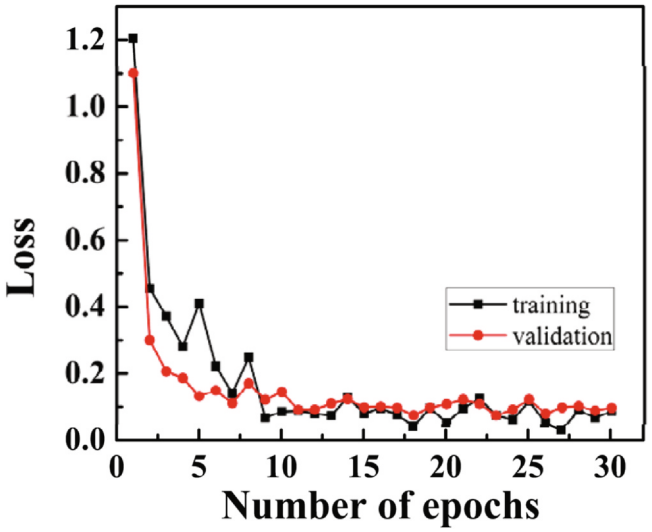

Fig. 8. RMSE as a function of the number of epochs (30) for the validation (red line) and training (black line) datasets using the following hyperparameters: batch size: 32; learning rate: 0.00001; SGDM optimizer. (For interpretation of the references to color in this figure legend, the reader is referred to the web version of this article.)

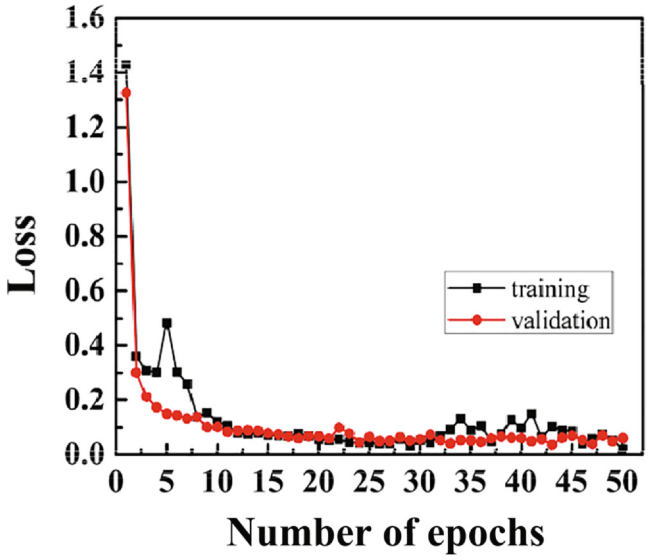

Fig. 9. RMSE as a function of the number of epochs (50) for the validation (red line) and training (black line) datasets using the following hyperparameters: batch size: 32; learning rate: 0.00001; SGDM optimizer). (For interpretation of the references to color in this figure legend, the reader is referred to the web version of this article.)

the composition of mixture stones. Fourth, dual energies in conventional CT were required to correctly differentiate pure uric acid stone, [15], however, using our method, pure uric acid stones could be differentiated using only a single energy.

Nevertheless, it should be noted that the CNN model developed in this study did not correctly classify a urinary stone image in the test dataset. In particular, one mixture stone (test image) was misclassified as a uric acid stone. Fig. 10 shows the mixture stone test image that was misclassified by our proposed model. Theoretically, a mixture stone has an effective atomic number (Z_{eff} ≈ 10–12) between that of the uric acid and calcium stones. In contrast, the uric acid stone (Z_{eff} ≈ 7) has a lower linear attenuation coefficient (small CT value, which appears as a dark color in CT images) than the other stones [30]. As shown in Fig. 10, some pixels show dark colors similar to uric acid (Fig. 2c), which could be the reason for the misclassification.

The acquisition parameters for urinary stones also influenced the performance of the model. Though the dataset was classified into three categories (calcium, mixture, and uric acid stones) based on mean CT value and EDX, the mean CT value is, in turn, influenced by tube voltage in the CT scan. A low source voltage (65 kV) could differentiate urinary stones into different categories in a relatively more effective manner [40]. Therefore, the optimized acquisition parameters for urinary stones are those listed in Table 1.

There are two limitations of this study. First, a larger number of

Table 4
Confusion matrix for the automated classification of urinary stones into three types.

		Predicted		
		Calcium	Mixture	Uric acid
Truth	Calcium	100% (243)	0	0
	Mixture	0	98.8% (80)	1.2% (1)
	Uric acid	0	0	100% (81)

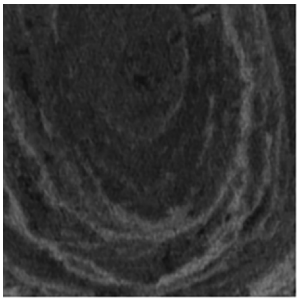

Fig. 10. Mixture stone micro-CT image misclassified by the proposed model.

urinary stones images is necessary to evaluate the classification accuracy of the final model. In clinical practice, automatic classification would be needed before treatment to identify the type of urinary stones within the human body. In our study, automatic classification was applied to urinary stones that had been removed via surgery. This preliminary study was conducted to obtain a correlation between the mean CT value and chemical compositions obtained via the EDX spectra. In future works, some investigations are needed to translate our findings into a clinically useful approach such as correlation HU values of urinary stones between in and vitro micro CT images and in-vivo clinical CT images. The automated classification will be used to classify urinary stones on an in-vivo study as test dataset.

5. Conclusions

In this study, an automated approach was developed for the classification of urinary stones into three types (calcium, uric acid, and mixture stones) based on micro-CT images of the stones. The proposed model yielded a test accuracy of 0.9959 with a classification error of 1.2%, which proved that our automated approach could accurately classify images of urinary stones images into the three types.

Acknowledgments

The authors are grateful for the support of Hasan Sadikin Hospital, Indonesia. We would also like to thank Kyushu University, Japan (Arimura Laboratory) for allowing us to use their Deep Learning server for this study. This study was financially supported by the Indonesia Endowment Fund for Education (LPDP), Enhancing International Publication Program (EIP) (T/1226/D3.2/KD.02.00/2019), and DIKTI (2/E1/KP.PTNBH/2020), Indonesia.

Appendix A. Supplementary data

Supplementary data to this article can be found online at https://doi.org/10.1016/j.ejmp.2020.09.007.

References

[1] Alelign T, Petros B. Kidney stone disease: an update on current concepts. 3068365 Adv Urol2018:1–2. https://doi.org/10.1155/2018/3068365.
[2] Cook medical. World Kidney Day: A global look at a growing concern. https://www.cookmedical.com/urology/world-kidney-day-a-global-look-at-agrowing concern/; 2016 [accessed 17 January 2019].
[3] Parakh A, Lee H, Lee JH, Eisner BH, Sahani DV, Do S. Urinary stone detection on CT images using deep convolutional neural networks: evaluation of model performance and generalization. Radiol Artif Intell 2019(1). https://doi.org/10.1148/ryai.2019180066. e180066.
[4] Chen Z, Prosperi M, Bird MY. Prevalence of kidney stones in the USA: the national health and nutrition evaluation survey. J Clin Urol 2019;12:296–302. https://doi.org/10.1177/2051415818813820.
[5] Kittanamongkolchai W, Vaughan LE, Enders FT, Dhondup T, Mehta RA, Krambeck AE, et al. The changing incidence and presentation of urinary stones over 3 decades. Mayo Clin Proc 2018;93:291–9. https://doi.org/10.1016/j.mayocp.2017.11.018.
[6] Barbas C, Garcia A, Saavedra L, Muros M. Urinary analysis of nephrolithiasis markers. J Chromatogr B 2002;781:433–55.
[7] Kidney Atlas. Remedies for the 5 most common types of kidney stones, https://www.kidneyatlas.org/the-5-most-common-types-of-kidney-stones/; 2018 [accessed 17 January 2019].
[8] Ranabothu S, Bernstein AP, Drzewiech BA. Diagnosis and management of non-calcium-containing stones in the pediatric population. Int Urol Nephrol 2018;50:1191–8. https://doi.org/10.1007/s11255-018-1883-0.
[9] European Association of Urology. Guidelines on urolithiasis, https://www.uroweb.org/guideline/urolithiasis/; 2017. [accessed 17 January 2019].
[10] Wisenbaugh ES, Paden RG, Silva AC, Humphhreys MR. Dual-energy vs conventional computed tomography in determining stone composition. Urology 2014;83:1243–7. https://doi.org/10.1016/j.urology.2013.12.023.
[11] Liden M. A new method for predicting uric acid composition in urinary stones using routine single energy. Urolithiasis 2018;46:325–33.
[12] Park HS, Gong MK, Yoon GY, Moon DG, Cheon J, Choi YD. Computed tomography-based novel prediction model for the outcome of shockwave lithotripsy in proximal ureteral stones. J Endourol 2016;30:810–6.
[13] Stewart G, Johnson L, Ganesh H, Davenport D, Smelser W, Crispen P, et al. Stone size limits the use of Housfield Units for prediction of calcium oxalate stone composition. Urology 2015;85:292–5.
[14] Fitri LA, Asyana V, Ridwan T, Anwary F, Soekersi H, Latief FDE, et al. Dual energy micro-CT Skyscan 1173 was able to characterize the composition of the urinary stone. J Phys: Conf Ser 2016;694:012053.
[15] Ananthakrishnan L, Duan X, Xi Y, Lewis MA, Pearle MS, Antonenlli JA, et al. Dual-layer spectral detector CT: non-inferiority assessment compared to dual-source dual energy CT in discriminating uric acid from non-uric acid renal stones ex vivo. Abdom Radiol 2018;43:3075–81.
[16] Black KM, Law H, Aldoukhi AH, Roberts WW, Deng J, Ghani KR. Deep learning computer vision algorithm for detecting kidney stone composition: towards an automated future. Eur Urol Suppl 2019;18:e853–4. https://doi.org/10.1016/S1569-9056(19)30624-4.
[17] Langkvist M, Jendeberg J, Thunberg P, Loutfi A, Liden M. Computer aided detection of ureteral stones in thin slice computed tomography volumes using convolutional neural networks. Comput Biol Med 2018;97:153–60. https://doi.org/10.1016/j.compbiomed.2018.04.021.
[18] Xiang H, Chen Q, Wu Y, Xu D, Qi S, Mei J, et al. Urine calcium oxalate crystallization recognition method based on deep learning. 2019 Int Conf Autom Comput Technol Manag (ICACTM);2019:30–33. https://doi.org/ 10.1109/ICACTM.2019.8776769.
[19] Kazemi Y, Mirroshandel SA. A novel method for predicting kidney stone type using ensemble learning. Artif Intell Med 2018;84:117–26. https://doi.org/10.1016/j.artmed.2017.12.001.
[20] Chaitanya SMK, Kumar PR. Detection of chronic kidney disease by using artificial neural networks and gravitational search algorithm. Innovations in electronics and communication engineering Singapore: Springer; 2019. p. 441–8. https://doi.org/10.1007/978-981-10-8204-7_44.
[21] De Perrot T, Hofmeister J, Burgermeister S, Martin SP, Feutry G, Klein J, et al. Differentiating kidney stones from phleboliths in unenhanced low-dose computed tomography using radiomics and machine learning. Eur Radiol 2019;29:4776–82. https://doi.org/10.1007/s00330-019-6004-7.
[22] Lee SC, Kim HK, Chun IK, Cho MH, Lee SY, Cho MH. A flat-panel detector based micro-CT system: performance evaluation for small-animal imaging. Phys Med Biol 2003;48:4173–85.
[23] Szewczykowski PP, Skarzynski L. Application of the X-ray micro-computed tomography to the analysis of the structure of polymetric materials. Polimery 2019;64:12–22. https://doi.org/10.14314/polimery.2019.1.2.
[24] Alexander SL, Rafaels K, Gunnarsson CA, Weerasooriya T. Structural analysis of the frontal and parietal bones of the human skull. J Mech Behav Biomed Mater 2019;90:689–701. https://doi.org/10.1016/j.jmbbm.2018.10.035.
[25] Fitri LA, Warty Y, Haryanto F, Fauzi U, Latief F. Optimization of imaging parameters in micro CT scanner based on signal-to-noise ratio for analysis of urinary stones composition. Iranian J Med Phys 2019.
[26] Wassilkowska A, Czaplicka-Kotas A, Bielski A, Zielina M. An analysis of the elemental composition of micro-samples using EDS technique. Chemia Zeszyt 2014;1:133–48. https://doi.org/10.4467/2353737XCT.14.283.3371.
[27] Wollman DA, Irwin KD, Hilton GC, Dulcie LL, Newbury DE, Martinis JM. High-resolution, energy-dispersive microcalorimeter spectrometer for X-ray microanalysis. J Microsc 1997;188:196–223.
[28] Kuhn M, Johnson K. Applied predictive modeling. 1th ed. New York: Springer; 2013.
[29] James G, Witten D, Hastie T, Tibshirani R. An introduction to statistical learning. New York: Springer; 2014.
[30] Machine Learning Mastery. What is the difference between test and validation datasets? Machine Learning Mastery. https://machinelearningmastery.com/difference-test-validation-datasets/; 2017 [accessed 25 October 2019].
[31] Russell SJ, Norvig P. Artificial intelligence: a modern approach. 3rd ed. Malaysia: Pearson Education; 2016.
[32] Shin HC, Roth HR, Gao M, Lu L, Xu Z, Nouges I, et al. Deep convolutional neural networks for computer-aided detection: CNN architectures, data set characteristics and transfer learning. IEEE Trans Med Imaging 2016;35:1285–98. https://doi.org/10.1109/TMI.2016.2528162.
[33] Menze BH, Jakab A, Bauer S, Cramer JK, Farahani K, Kirby J, et al. The multimodal brain tumor image segmentation benchmark (BRATS). IEEE Trans Med Imaging 2015;34:1993–2024. https://doi.org/10.1109/TMI.2014.2377694.
[34] Bar Y, Diamant I, Wolf L, Lieberman S, Konen E, Greenspan H. Chest pathology detection using deep learning with non-medical training. Proc. IEEE 12th Int. Symp Biomed Imag 2015. p. 294–7. https://doi.org/10.1109/ISBI.2015.7163871.

[35] Shen W, Zhou M, Yang F, Yang C, Tian J. Multi-scale convolutional neural networks for lung nodule classification. Int Conf Inf Process Med Imaging 2015;24:588–99. https://doi.org/10.1007/978-3-319-19992-4_46.
[36] Wolterink JM, Leiner T, de Vos BD, van Hamersvelt RW, Viergever MA, Išgum I. Automatic coronary artery calcium scoring in cardiac CT angiography using paired convolutional neural networks. Med Imag Anal 2016;34:123–36. https://doi.org/10.1016/j.media.2016.04.004.
[37] Dwork C, Feldman V, Hardt M, Pitassi T, Reingold O, Roth A. Generalization in Adaptive Data Analysis and Holdout Reuse. Neural Information Processing Systems (NIPS) 2015.
[38] Moons KG, Altman DG, Reitsma JB, Ioannidis JP, Macaskill P, Steyerberg EW, et al. Transparent Reporting of a multivariable prediction model for Individual Prognosis or Diagnosis (TRIPOD): explanation and elaboration. Ann Intern Med 2015;162(1):W1–73.
[39] Miernick A, Eilers Y, Bolwien C, Lambrecht A, Hauschke D, Rebentisch G, et al. Automated analysis of urinary stone composition using Raman spectroscopy: pilot study for the development of a compact portable system for immediate post-operative ex vivo application. J Urol 2013;190:1895–900. https://doi.org/10.1016/j.juro.2013.06.024.
[40] Poletti PA, Platon A, Rutschmann OT, Schmidlin FR, Iselin CE, Becker CD. Low dose versus standard dose CT protocol in patients with clinically suspected renal colic. Am J. Roentgenol 2007;188:927–33.